A MIXED FLOWING/POWDER SNOW AVALANCHE MODEL

P.A. Bartelt* M.A. Kern and M. Christen
Swiss Federal Institute of Snow and Avalanche Research (SLF), CH-7260 Davos, Switzerland

ABSTRACT One-dimensional layer-averaged equations describing the mechanics of mixed flowing/powder snow avalanches are formulated and solved. The equations describe the volume, mass and momentum balance of the powder and flowing parts of the avalanche. The powder cloud of changing density is assumed to be incompressible and the suspended ice particles inert with respect to small scale turbulent fluctuations in the air. Normalized velocity and density profiles are based on experiments and supplement the depth-averaged equations. The dense flowing avalanche is of constant flow density. Longitudinal straining of the granular flow mass is formulated with an active/passive pressure with cohesion. The mass exchange between the flowing and powder avalanche is assumed to be velocity dependent. Air entrainment into the powder cloud is governed by a dimensionless form factor. Therefore, the initiation and eventual self-acceleration of the powder cloud from a full flowing avalanche is modelled. It is possible to simulate the evolution of a large powder cloud from a dense flowing avalanche. Deceleration of the powder cloud is due to conversion of kinetic flow energy into potential energy and turbulent energy in the air which is eventually dissipated. The stagnant powder cloud left behind the flowing parts is modelled as a mass loss at the tail of the avalanche. Several calculation examples of mixed flowing/powder avalanches are presented showing the practicality of the new model.

1 INTRODUCTION

Directly after the catastrophic avalanche winter of 1999, the SLF began appraising hazard maps where extreme avalanche events occurred (Gruber & Margreth 2000). A detailed assessment of several maps in the Obergoms region, Canton Wallis, is contained in these proceedings (Gruber & Bartelt 2000). One of the important findings of these appraisals was the present inability of avalanche practitioners to model the behavior of mixed flowing/powder snow avalanches. In 1999, powder clouds often flowed farther than expected and powder snow avalanche deposits redirected the flow direction of subsequent flowing avalanches, often with severe side effects (Gruber & Margreth 2000). The avalanche winter of 1999 clearly showed that a simple mixed flowing/powder snow avalanche dynamics model is failing in practice.

Models to predict the motion of a powder snow cloud have been proposed by different researchers (for an overview, see (Hutter 1996)). These models range from simple Voellmy-type hydraulic models (Voellmy 1955), to depth-integrated models founded on turbidity current theory (Parker, Fukushima, & Pantin 1986). Of course, models based on the solution of the full three-dimensional Navier-Stokes equations (Sampl 1998) have also been proposed. These models have found widespread application primarily in Austria, but also in Switzerland (Issler 1998).

Each modelling concept can be criticized. For example, Voellmy-type models are judged too simple to accurately represent the complex flow behavior of powder snow avalanches. They are, however, well liked by practitioners. The depth-averaged turbidity concept considers entrainment and deposition processes but has not been applied to model more than one real powder snow avalanche event (Fukushima & Parker 1990). Full three-dimensional models have not yet been coupled to flowing avalanche models. In addition, they are both computationally demanding and expensive. Few practitioners have the know-how, the money or the computer infrastructure to apply them to real situations.

Despite these modelling attempts, however, the greatest hindrance to the development of a mixed flowing/powder snow avalanche model is the lack of experimental data. The Swiss Valle de la Sionne test site was constructed to remedy this problem (see the paper in these proceedings). For an example of an powder avalanche in this experimental area, see Figure 1. Although the test site was partially destroyed during the catastrophic avalanche winter of 1999, enough data was gathered, especially photogrammetric mass balance measurements and video recordings, to begin the development of a more complicated avalanche dynamics model. Work is presently underway to rebuild the test site.

In the following, a mixed flowing/powder avalanche model is presented.

The motion of the powder cloud is described by a set of depth-integrated balance equations for volume, mass and momentum. The incompressible, turbulent powder cloud is assumed to be composed of ice particles suspended in air to form a continuous multi-phase

*Corresponding author address: Perry Bartelt, Swiss Federal Institute of Snow and Avalanche Research, Flüelastr. 10, CH-7260 Davos Dorf;tel +41 81 4170 251; fax +41 81 4170 110; email bartelt@slf.ch

Figure 1: *Powder avalanche in the Vallée de la Sionne test site, Feb 30, 1999. Note the large motionless powder cloud at the tail of the avalanche. At this point, the avalanche is moving at approximately 40 ms^{-1} and the flow heights at the avalanche head are about 10m.*

medium of variable density. Velocity and density profiles over the height of the flow are assumed.

The flowing avalanche is presently considered to move in a dense plug of constant density, which undergoes longitudinal tensile (active) and compressive (passive) straining. The shear strains are considered to be concentrated at the base of the flow.

The combined model differs from previous efforts to simulate mixed avalanche flow in the following:

1. We parameterize the mass exchange between the flowing and powder parts. Thus, it is possible to initiate a powder avalanche from a flowing avalanche core. Our motivation is to simplify the specification of the initial conditions for practitioners, who prefer to specify a fracture slab of known length, width and height. The alternative would be to specify a powder cloud of known density, height and velocity. If the mass exchange coefficient is set to zero, a full flowing avalanche without a powder cloud is modelled.

2. An inspection of Valle de la Sionne videos shows that a powder snow avalanche leaves behind a motionless cloud. Because of turbulence, the height of this *stagnant* cloud increases, but as more turbulent energy is dissipated, the stagnant cloud eventually settles. We include the stagnant powder cloud in the model. Although it has no destructive force, mass is removed from the moving cloud, influencing its behavior. The settling of the stagnant cloud, however, is not yet included in the model.

3. One essential aspect of powder snow avalanche modelling is correctly accounting for the frictional forces acting on the cloud. We derive these forces by balancing the potential and kinetic energies of the cloud (see Section 3). A rise in the cloud height (a rise of the cloud's center of mass) is compensated by a reduction in the cloud's translational kinetic energy. Also, the energy required to accelerate entrained mass from the incumbent snowcover or from the flowing avalanche is accounted for, causing a direct reduction of the cloud's kinetic energy. This approach differs significantly from the turbidity current model of Parker (Parker, Fukushima, & Pantin 1986), who accounted for such processes by reducing the *turbulent* kinetic energy of the cloud, and not the *translational* kinetic energy. This procedure simplifies the model significantly, because we do not explicitly need to track the turbulent kinetic energy. Instead, only a turbulent drag is considered. The motivation is to avoid the use of a complicated turbulence model, which requires greater computational resources. Furthermore, the closure problem is avoided.

4. Until now, simple powder snow avalanche models have been solved by assuming stationary or equilibrium flow conditions. The task of solving a highly complex system of instationary equations - considering both mass and air entrainment - requires stable numerical schemes. As a first step, we are interested in the application of numerical procedures, which are valid for a wide range of parameters. For this reason, we briefly discuss the solution of the powder snow avalanche equations using upwinded finite difference schemes.

5. The model for the dense flowing avalanche is presented in (Bartelt, Salm, & Gruber 1999) and will not be discussed in detail. The equations will merely be stated. The model has been extended to simulate the entrainment of the snowcover at the avalanche head. Also, cohesion has been included in the active-passive pressure formulation.

2 STATEMENT OF DIFFERENTIAL EQUATIONS

The depth-averaged governing differential equations for mixed avalanche flow are stated below. The meaning of each symbol is listed in Table 1.

Mass conservation (flowing core):

$$\partial_t \tilde{h}_f + \partial_s(\tilde{h}_f U_f) = \dot{S}_e + \dot{S}_d - \dot{S}_f, \qquad (1)$$

Momentum conservation (flowing core):

$$\begin{aligned} &\partial_t(\tilde{h}_f U_f) + \partial_s(\tilde{h}_f U_f^2) + \tfrac{1}{2}\partial_s(\lambda \tilde{h}_f^2) = \\ &\quad g\tilde{h}_f \sin\alpha - \mu g \tilde{h}_f \cos\alpha - g\frac{U^2}{\xi h_f}\tilde{h}_f - \frac{c\tilde{h}_f}{\rho_f h_f} \\ &\quad -\tfrac{1}{2}\frac{(\rho_s-\rho_a)}{\rho_f}\dot{S}_e U_f + \tfrac{1}{2}\frac{(\rho_s-\rho_a)}{\rho_f}\dot{S}_e(h_s - h_f)\frac{g}{U_f} \end{aligned} \qquad (2)$$

with

$$\lambda = \begin{cases} \frac{1}{w}\left(k_p g\cos\alpha + \frac{4c\sqrt{k_p}}{\rho_f h_f}\right): & \frac{\partial U_f}{\partial s} \le 0 \quad \text{(passive)} \\ \frac{1}{w}\left(k_a g\cos\alpha - \frac{4c\sqrt{k_a}}{\rho_f h_f}\right): & \frac{\partial U_f}{\partial s} > 0 \quad \text{(active)} \end{cases} \qquad (3)$$

The primary modelling assumptions of the flowing core are:

1. The granular flowing core is a fluid continuum of constant density, ρ_f.
2. The flow width $w(s)$ is known.
3. A clearly defined flow surface exists between the flowing core and the powder cloud. The height of this flow surface is $h_f(s,t)$, which is the average flow height across the width of flow.
4. The vertical pressure distribution is hydrostatic. Centripetal pressures, which modify the hydrostatic pressure distribution, are not accounted for.
5. The velocity U_f is the mean depth-averaged velocity. The velocity profile is rectangular, meaning that no shear strains or strain rates exist in the flow body. Shearing is concentrated at the base of flow. The basal shear stress τ_b is

$$\tau_b = c + \mu\sigma_z + \frac{\rho_f g}{\xi} U_f^2, \qquad (4)$$

where σ_z is the overburden stress, $\sigma_z = \rho_f g h_f \cos\alpha$; μ is the coefficient of dry friction; ξ is the velocity dependent drag coefficient and c is the cohesion of the granular mass. We therefore assume a so-called Voellmy drag with cohesion.

6. The flowing core undergoes longitudinal straining. The stress in the longitudinal direction, σ_s, is proportional to the hydrostatic pressure and is given by

$$\sigma_s = k\sigma_z, \qquad (5)$$

where k is active-passive pressure coefficient. Active (k_a) and passive (k_p) coefficients are determined by the sign of the velocity gradient in the flow direction $\frac{\partial U_f}{\partial s}$:

$$\begin{aligned} k &= k_a \quad \text{for} \quad \tfrac{\partial U_f}{\partial s} > 0, \\ k &= k_p \quad \text{for} \quad \tfrac{\partial U_f}{\partial s} \leq 0. \end{aligned} \qquad (6)$$

Rankine's theory with cohesion is applied to determine the active-passive coefficients (Bartelt, Salm, & Gruber 1999).

7. The final two terms on the right-hand side of the momentum equation account for snow entrainment. The first term represents the deceleration caused by accelerating the snow mass up to the avalanche flow velocity; the second term represents the deceleration caused by lifting the entrained snow mass into the flowing core (potential energy). The volumetric entrainment rate per unit flow length is $\dot{S}_e$ [$\mathrm{m^2 s^{-1}}$]. Therefore, the mass entrianment rate is $\rho_s \dot{S}_e$ where ρ_s is the density of the entrained snow.
8. The volume of snow per unit flow length per unit time ejected by the flowing core into the powder avalanche is $\dot{S}_f$. The mass ejection rate is $\dot{m}_f = \rho_f \dot{S}_f$.

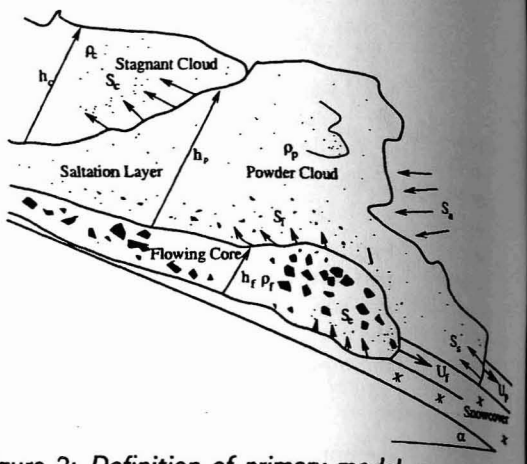

Figure 2: *Definition of primary model parameters for mixed avalanche model. An avalanche consists of a flowing core and a moving powder and motionless stagnant cloud.*

The depth-averaged equations for the powder cloud are:

Volume conservation (powder cloud):

$$\partial_t \tilde{h}_p + \partial_s(\tilde{h}_p U_p) = \dot{S}_a + \dot{S}_f + \dot{S}_s - \dot{S}_d - \dot{S}_c, \qquad (7)$$

Mass conservation (powder cloud):

$$\begin{aligned} &\partial(\rho_p \tilde{h}_p) + \beta_1 \partial_s(\rho_p \tilde{h}_p U_p) = \\ &\quad \rho_a \dot{S}_a + \rho_f \dot{S}_f + \rho_s \dot{S}_s - \rho_d \dot{S}_d - \rho_p \dot{S}_c \end{aligned} \qquad (8)$$

Momentum conservation (powder cloud):

$$\begin{aligned} &\beta_1 \partial_t(\rho_p \tilde{h}_p U_p) + \beta_2 \partial_s(\rho_p \tilde{h}_p U_p^2) + \tfrac{1}{2}\partial_s\left[\tfrac{\rho_p g}{w}\cos\alpha \tilde{h}_p^2\right] \\ &= g(\rho_p - \rho_a)\tilde{h}_p \sin\alpha - \tfrac{1}{2}\rho_a \dot{S}_a U_p \\ &+ \tfrac{1}{2}\rho_f \dot{S}_f \tfrac{(U_f^2 - U_p^2)}{U_p} \\ &- \tfrac{1}{2}\rho_f \dot{S}_f \tfrac{g}{U_p}(h_f + h_p) - \tfrac{1}{2}(\rho_s - \rho_a)\dot{S}_s U_p \\ &+ \tfrac{1}{2}(\rho_s - \rho_a)\dot{S}_s \tfrac{g}{U_p}(h_s - h_p) \\ &- \tfrac{T_e}{2}\rho_p \tilde{h}_p g \tfrac{\dot{h}_p}{U_p} \\ &- c_T \rho_p U_p^2 w + \tfrac{1}{2}\rho_p \dot{S}_c U_p. \end{aligned} \qquad (9)$$

The primary modelling assumptions are:

1. The powder cloud is assumed to be a multi-phase continuum of variable density,

$$\rho_p = \theta_i \rho_i + \theta_a \rho_a = \theta_i \rho_i + (1 - \theta_i)\rho_a \qquad (10)$$

where θ_i and θ_a are the volumetric contents of the ice and air respectively; ρ_i and ρ_a are the densities

of ice and air. The suspended ice particles and the surrounding air move with the same mean velocity and thus are described by a single momentum equation.

2. Density variations of the powder cloud arise due to changes in the amount of suspended ice particle per unit volume. The air and ice phases are incompressible.

3. The turbulent drag is governed by the coefficient C_t:
$$\tau_t = C_t U_p^2. \tag{11}$$
Viscous drag is neglected.

4. The mean downslope velocity U_p in the direction s is much larger than the velocity component in the direction perpendicular to the slope. The mean pressure $p(z,t)$ inside the powder cloud is assumed to be hydrostatic,
$$p(s,t) = \rho_p(s,t) g (h_p(s,t) - z) \tag{12}$$
where h_p is the height of the snow cloud.

5. The flow is homogeneous in the lateral direction, i.e. there are no variations of the flow field in the lateral direction. The velocity in this direction is zero.

6. The motion of the powder cloud is turbulent. The velocity field $\tilde{u}_p$ consists of a mean velocity u_p which is overlayed with turbulent fluctuations, u_p':
$$\tilde{u}_p = u_p + u_p', \qquad u_p = \langle \tilde{u}_p \rangle \tag{13}$$
Here, $\langle \tilde{u}_p \rangle$ denotes a spatial averaging over the velocity field. We make the further assumption that, within our mulitphase flow, the ice particles are inert with respect to the small scale turbulent motion of the air. This implies that the concentration of snow particles is not subject to small scale turbulent fluctuations so that
$$\tilde{\theta}_i \approx \langle \tilde{\theta}_i \rangle = \theta_i. \tag{14}$$
Subsequently,
$$\rho_p = \langle \tilde{\rho}_p \rangle = \theta_i \rho_i + (1 - \theta_i) \rho_a. \tag{15}$$
The density is not subject to small scale turbulent fluctuations.

7. According to results of physical powder cloud modelling (Keller 1996), we assume that the density varies linearly and the velocity parabolically over the flow height (see Fig. 3):
$$\rho_p(z,t) = (\rho_0 - \rho_a)\left(1 - \frac{z}{h_p}\right) + \rho_a \tag{16}$$
and
$$u_p(z,t) = u_0 \left(1 - \left(\frac{z}{h_p}\right)^2\right). \tag{17}$$

8. The mean density and velocity of the powder cloud are given by
$$\rho_p = \frac{1}{h_p}\int_0^{h_p} \rho_p(z,t)\,dz = \frac{1}{2}(\rho_0 + \rho_a) \tag{18}$$
and
$$U_p = \frac{1}{h_p}\int_0^{h_p} u_p(z,t)\,dz = \frac{2}{3}u_0. \tag{19}$$
With these assumptions, depth-averaging of the differential equations leads to the following profile form factors
$$\beta_1 = \frac{1}{4}\left(\frac{5\rho_p + 3\rho_a}{\rho_p + \rho_a}\right) \tag{20}$$
and
$$\beta_2 = \frac{3}{20}\left(\frac{11\rho_p + 5\rho_a}{\rho_p + \rho_a}\right) \tag{21}$$
For more information concerning depth-averaging and profile factors see (Savage & Hutter 1991).

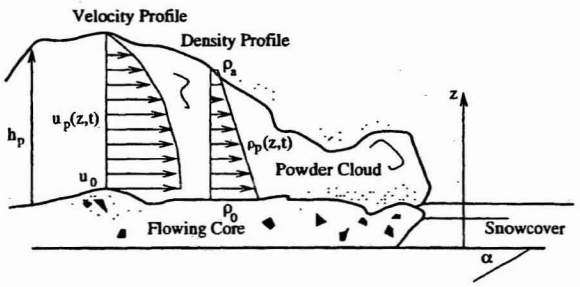

Figure 3: *Velocity and density profiles in powder cloud*

3 POWDER CLOUD DRAG

The deceleration of the powder cloud is derived using a simple energy analysis. Consider Fig. 4, which shows a section of an idealized powder cloud at time t_0 and time $t_1 = t_0 + \Delta t$. Between the two time periods, the cloud entrains air, snow from the flowing core and snow from the snowcover. The cloud increases in mass and height.

Let Δm_a be the amount of air mass entrained within the time period Δt. Similarly, Δm_s and Δm_f are the amounts of snowcover mass and granular flowing mass entrained into the powder cloud.

The conservation of potential and kinetic energy between the times t_0 and t_1 leads to
$$\begin{aligned} &\tfrac{1}{2}m_0 U_0^2 + \tfrac{1}{2}m_0 g h_0 + \tfrac{1}{2}\Delta m_f U_f^2 - \tfrac{1}{2}\Delta m_f g h_f \\ &\quad + \tfrac{1}{2}\Delta m_a g h_0 + \tfrac{1}{2}\Delta m_s g h_s \\ &= \tfrac{1}{2}m_1 U_1^2 + \tfrac{1}{2}m_1 g h_1. \end{aligned} \tag{22}$$
Noting that
$$U_1 = U_0 + \Delta U \tag{23}$$

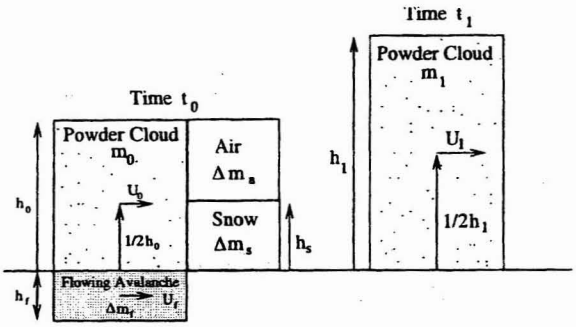

Figure 4: *Energy analysis to determine powder cloud drag*

$$h_1 = h_0 + \Delta h \tag{24}$$

$$m_1 = m_0 + \Delta m = m_0 + \Delta m_a + \Delta m_f + \Delta m_s \tag{25}$$

and solving the balance equation for $m_0 \frac{\Delta U}{\Delta t}$ (the change in momentum) leads to the following expression for the deceleration of the powder cloud:

$$\begin{aligned} m_0 \tfrac{\Delta U}{\Delta t} = \tfrac{1}{U_0}[&\tfrac{1}{2}(\dot{m}_s + \dot{m}_f + \dot{m}_a)U_0^2 \\ &+\tfrac{1}{2}\dot{m}_s g(h_s - h_0) - \tfrac{1}{2}\dot{m}_f g(h_f + h_0) \\ &+\tfrac{1}{2}\dot{m}_f U_f^2 - \tfrac{1}{2}m_0 g\dot{h}]. \end{aligned} \tag{26}$$

Each one of the terms in the above equation translates directly into a drag contribution in the momentum balance equation:

Air Entrainment

$$m_0 \frac{\Delta U}{\Delta t} = -\frac{1}{2}\dot{m}_a U_0 = -\frac{1}{2}\rho_a \dot{S}_a U_p \tag{27}$$

Snow Entrainment

$$\begin{aligned} m_0 \tfrac{\Delta U}{\Delta t} &= -\tfrac{1}{2}\dot{m}_s U_0 + \tfrac{1}{2}\dot{m}_s \tfrac{g}{U_0} g(h_s - h_0) \\ &= -\tfrac{1}{2}(\rho_s - \rho_a)\dot{S}_s U_p + \\ &\quad \tfrac{1}{2}(\rho_s - \rho_a)\tfrac{g}{U_p}(h_s - h_p) \end{aligned} \tag{28}$$

Flowing/Powder Mass Exchange

$$\begin{aligned} &m_0 \tfrac{\Delta U}{\Delta t} = \tfrac{1}{U_0}\left[\tfrac{1}{2}\dot{m}_f U_f^2 - \tfrac{1}{2}\dot{m}_f U_0^2 - \tfrac{1}{2}\dot{m}_f g(h_f - h_0)\right] \\ &= -\tfrac{1}{2}\rho_f \dot{S}_f \left(\tfrac{U_f^2 - U_p^2}{U_p}\right) - \tfrac{1}{2}\rho_f \dot{S}_f \tfrac{g}{U_p}(h_f - h_0) \end{aligned} \tag{29}$$

Potential/Kinetic Energy Exchange

$$m_0 \frac{\Delta U}{\Delta t} = -\frac{1}{2}m_0 g \frac{\dot{h}}{U_0} = -\frac{T_e}{2}\rho_p \tilde{h}_p \frac{\dot{h}_p}{U_p} \tag{30}$$

In the energy exchange coefficient, the factor T_e has been introduced to control the amount of energy dissipitation. If $T_e = 1$, then every unit change in potential energy, essential the increase in powder snow height, corresponds to an equal reduction in translational kinetic energy, that is, the avalanche flow velocity. A similar procedure was employed by (Fukushima & Parker 1990). However, in their formulation, an increase in cloud height was accompanied by a corresponding decrease in turbulent kinetic energy.

The mass entrainment rates are expressed in terms of the dimensionless parameters, E_a, E_f and E_s:

$$\dot{S}_a = E_a f(\tilde{h}_p, U_p, \rho_p) \tag{31}$$

$$\dot{S}_s = E_s f(\tilde{h}_p, U_p, \rho_p) \tag{32}$$

$$\dot{S}_f = E_f f(\tilde{h}_p, U_p, \rho_p). \tag{33}$$

The function $f(\tilde{h}_p, U_p, \rho_p)$ represents some function of the state variables. In summary, the motion of the powder cloud is defined by five parameters: E_a, E_s, E_f, C_t and T_e. We also stipulate, that mass is not ejected from the flowing avalanche until its speed reaches the thresh-hold velocity, U_t.

4 NUMERICAL SOLUTION OF GOVERNING EQUATIONS

The numerical solution of the flowing avalanche equations has been presented in detail in (Sartoris & Bartelt 2000). Therefore, in the following, we will be presenting the solution of the three equations governing the motion of the powder cloud.

The governing system of equation can be written in vectorial form as

$$\partial_t \vec{U} + \partial_s \vec{F} = \partial_t \vec{U} + A\partial_s \vec{U} = \vec{G}, \tag{34}$$

where

$$\begin{aligned} \vec{U} &= (\tilde{h}_p, \rho_p \tilde{h}_p, \rho_p \tilde{h}_p U_p)^T \\ \vec{F} &= (\tilde{h}_p U_p, \rho_p \tilde{h}_p U_p, \rho_p \tilde{h}_p U_p^2 + \frac{1}{2}\lambda \tilde{h}_p^2) \end{aligned} \tag{35}$$

with $\lambda = \frac{1}{w}\rho_p g \cos\alpha$. The vector $\vec{G}$ represents the right-hand sides of the differential equations (7), (8) and (9). The matrix A is

$$A = \begin{pmatrix} U_p & 0 & 0 \\ 0 & 0 & \beta_1 \\ 0 & -\beta_2 U_p^2 + \lambda \tilde{h}_p & 2\beta_2 U_p \end{pmatrix}. \tag{36}$$

Let $S^{-1}AS = \Lambda$, where Λ is a diagonal matrix with the eigenvalues of A. Then $S^{-1}A = AS^{-1}$ and

$$S^{-1}\partial_t \vec{U} + \Lambda S^{-1}\partial_s \vec{U} = S^{-1}\vec{G}. \tag{37}$$

First and second order upwinded finite difference schemes are then applied to the diagonalised system (37). The eigenvalues of A are:

$$\Lambda = (e_1, e_2, e_3) \tag{38}$$

where

$$e_1 = U_p, \tag{39}$$

$$e_2 = \beta_2 U_p + \sqrt{\beta_2^2 U_p^2 - \beta_1 \beta_2 U_p^2 + \beta_1 \lambda \tilde{h}_p} \quad (40)$$

and

$$e_3 = \beta_2 U_p - \sqrt{\beta_2^2 U_p^2 - \beta_1 \beta_2 U_p^2 + \beta_1 \lambda \tilde{h}_p}. \quad (41)$$

For more details see (Sartoris & Bartelt 2000).

5 EXAMPLE CALCULATIONS

In a first example calculation, we back-calculate an avalanche event captured at the Vallee de la Sionne field test site. Video and radar measurements recorded that the avalanche reached a velocity of 55 ms^{-1} as it passed the measurement pylon. The avalanche reached a maximum velocity of 70 ms^{-1} before running up the opposing slope, over-running the concrete bunker containing the radar. The powder cloud heights at the end of the event were well over 100m.

Based on photogrammetric measurements of the starting zone, we specified a 3.0m high fracture slab of mean density 300 kgm^{-3}. The width and length of the slab were approximately equal, 200m and 255m, respectively. The initial volume of the event was 150,000m^3.

The friction parameters of the flowing avalanche were set to the recommended values of the Swiss guidelines for numerical calculations, (Bartelt, Salm, & Gruber 1999): μ=0.16 and $\xi = 2500 ms^{-2}$. At the time of this particular event, the temperatures were low, the snow dry, and thus we specified $c = 0$ Pa, that is, no cohesion. The flowing avalanche also entrained a light ($\rho_s = 100$ kgm^{-3}) snowcover during it's downward motion.

The flowing avalanche accelerated quickly to a flow velocity of 45 ms^{-1}. A powder cloud developed rapidly. Already after 5s, a small, 0.5 m high saltation layer was predicted to flow above the core. By 20s, this saltation layer had grown to a powder cloud of 5 m with a density of 60 kgm^{-3}. This process is depicted in Fig. 5 and Fig. 6.

After running 700m, the mass loss of the flowing core became significant and the avalanche began to decelerate. At the same time, the powder cloud accelerated, eventually moving faster than the flowing avalanche, see Fig. 7. The powder avalanche reached a velocity of 57ms^{-1}, which aggrees well with measurements. In addition, the front flow height of the powder cloud was 18m, which also agrees well with video recordings.

The powder avalanche continued to accelerate and reached a terminal velocity of 70 ms^{-1} before running up the opposing slope, see Fig. 8.

Note that at the start of the event, the powder cloud is moving slower than the flowing avalanche. Perhaps the acceleration of the powder avalanche is too slow. An explanation for this behavior is that the momentum exchange between the flowing core and powder cloud is not yet correct. The sudden decrease in flowing

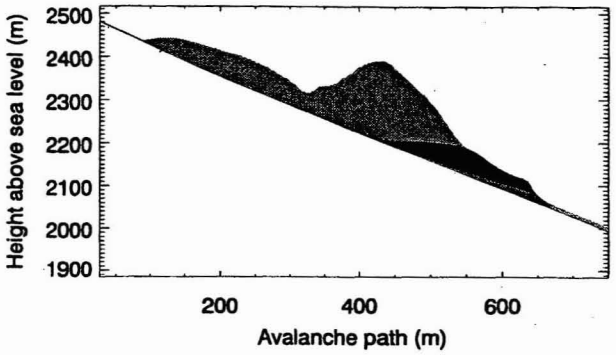

Figure 5: *Initiation of powder cloud. The flowing avalanche has been underway for 20 seconds.*

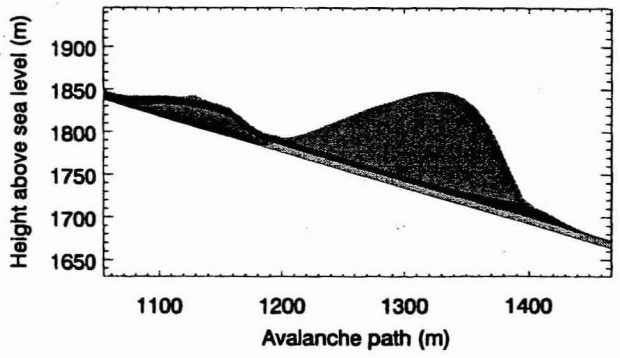

Figure 6: *The powder cloud is now moving faster than the flowing avalanche. Situation 40 seconds after release.*

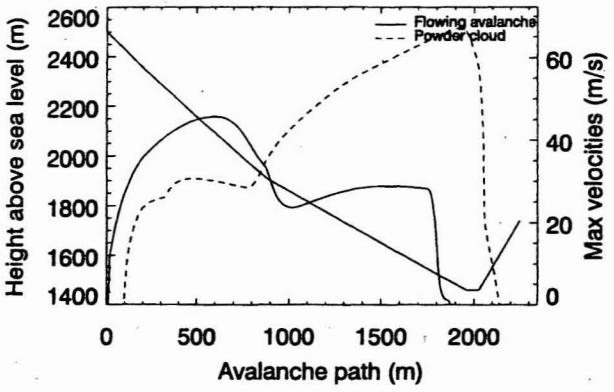

Figure 7: *Maximum flow velocity of the flowing and powder snow avalanche. In the beginning, the powder avalanche is slower than the flowing core. However, it eventually overtakes the core, reaching a maximum velocity very close to the measurements.*

avalanche velocity and the sudden increase in powder cloud velocity does not seem realistic.

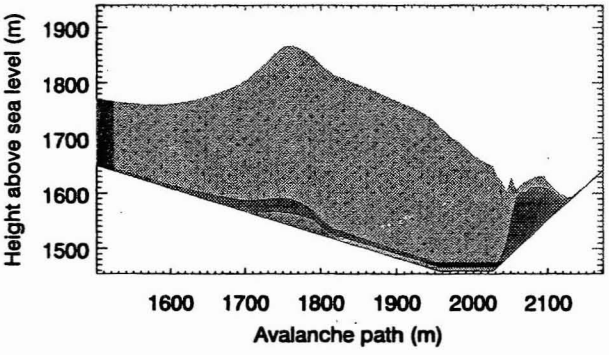

Figure 8: *The simulated avalanche running up the opposing slope. The powder cloud height is 100m. The stagnant cloud height is 250m. The clouds are drawn to scale. Situation after 65 seconds.*

The maximum densities of the powder cloud are depicted in Figure 9. In the acceleration zone, the densities are near 80 kgm^{-3}. These maximum densities arise as the powder cloud is beginning to form, that is, when the flow heights are small. In this sense, they can be considered saltation layer densities. When the cloud is fully developed at the valley bottom, the maximum densities are less than 20 kgm^{-3}. The cloud height is 100m, see Fig.10.

The stagnant cloud height is over 200m, which is too large. However, considering the fact that no settling or no energy dissipitation is included in the model, these

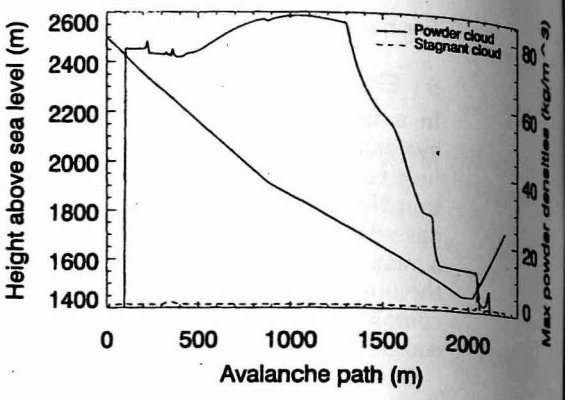

Figure 9: *Maximum flow density of the powder cloud. Densities of over 80 kgm^{-3} are obtained when the flow heights of the powder cloud are small.*

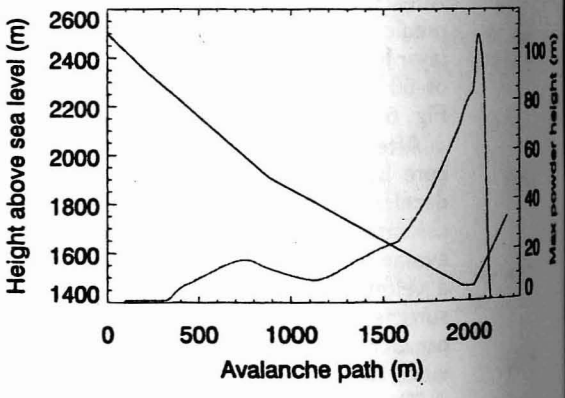

Figure 10: *Maximum height of the powder cloud. In the acceleration zone the predicted and measured flow heights agree.*

heights are certainly realistic.

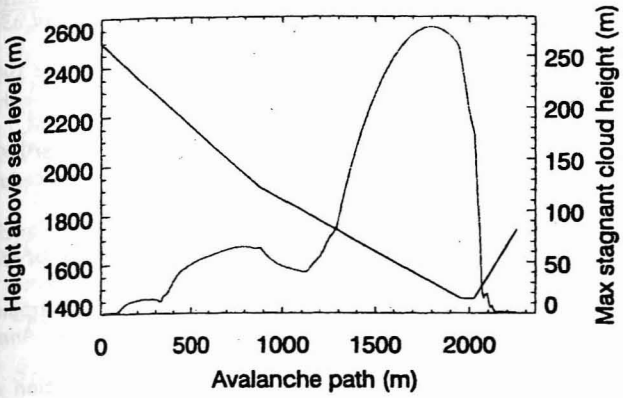

Figure 11: *Maximum height of the powder cloud. In the runup zone the stagnant cloud height is over 200m. This is clearly too high; however, settling and energy dissipitation in the cloud are not considered.*

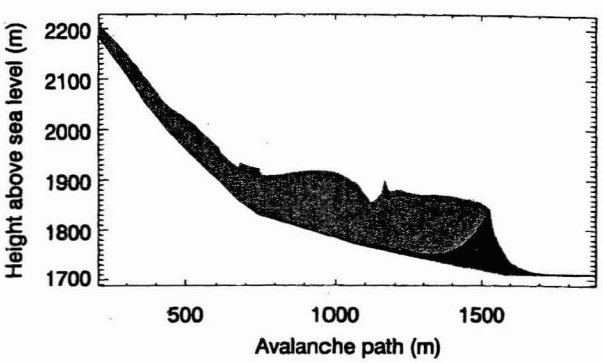

Figure 12: *The simulated powder cloud, stagnant cloud and flowing avalanche deposits at Samedan. The cloud has not begun to settle.*

The second avalanche event we investigate is the Samedan avalanche of 1951. This event is one of the calculation examples of the Swiss guidelines and is often used to validate avalanche dynamics calculations. The reason why it is included in our analysis is because it contains a long flat runout zone, unlike the Vallee de la Sionne avalanche.

The parameters of the previous calculation where changed slightly. Specifically, the air entrainment coefficient was doubled. In addition, the potential/kinetic energy transfer coefficient was increased from T_e=0.05 to T_e=0.25. The final simulated flow heights and runout distances of both the flowing avalanche and powder cloud are shown in Fig 12. For this case, the powder avalanche ran an additional 400 m past the flowing avalanche deposits. The predicted flow velocities are displayed in Fig 13.

In this example calculation, the flowing and powder parts have similar velocities after release. However, the powder cloud eventually passes the core, entering the runout zone independently. The same parameter combination can be used to simulate the Vallee de la Sionne avalanche, however, the resulting flow velocities are much smaller than measured.

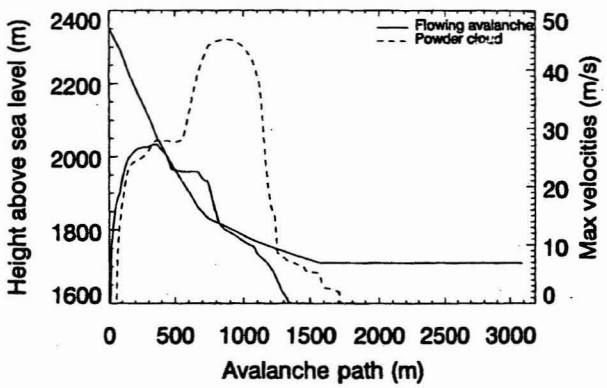

Figure 13: *Predicted maximum flow velocities. Note that the flowing and powder avalanches are in equilibrium before the powder cloud accelerates away from the core reaching a velocity of over 50ms^{-1} .*

6 CONCLUSIONS

In this paper, we have presented a system of depth-averaged equations describing the motion of mixed flowing/powder snow avalanches. The model includes the uptake of snow from the snowcover into the flowing core, the mass ejection from the flowing core into the powder cloud, the entrainment of air into the powder cloud and finally the discharge of powder from the downward moving turbulent cloud into a stagnant dust cloud located behind the avalanche front. The drag of

each mass exchange process was derived using a simple energy analysis.

With this model it was possible to:

1. Initiate a powder avalanche from a flowing avalanche. This is an important first step in introducing a powder snow avalanche model in practice, since only the fracture dimensions of the snow slab must be specified. This process avoids estimating the initial physical properties (initial density, velocity or height) of a powder snow avalanche.

2. Depending on the mass entrainment coefficients, primarily the air entrainment coefficient, the powder cloud can accelerate to higher velocities than the flowing core, disengage from the core and eventually move independently from the core forwards. Large runout distances can be obtained.

3. The mean density of the powder cloud was determined as snow mass was being ejected from the flowing avalanche. We found maximum densities of 100 kgm^{-3}, when the cloud was not very high. As more air was entrained into the cloud and as the cloud ran out, independently from the flowing avalanche, lower densities of the order 20 kgm^{-3} were predicted.

4. From a fracture slab of 2m, it was possible to generate powder and stagnation cloud heights of well over 100m. These heights, which correspond well to observations, are generated by air entrainment. Note also that these heights were generated within the framework of a depth-averaged model where the drag coefficients are based on the conservation of potential and kinetic energies.

Obviously, more work on the model is required. For example, the mass exchange processes are governed by dimensionless coefficients that are constant for an entire simulation. This is clearly a too simple assumption. Also the assumptions regarding the velocity and density profiles have not been validated by field experiments. On-going field tests at the Swiss Vallee de la Sionne test site should remedy this situation. Complicated mass balance measurements coupled with velocity and flow height measurements are now being performed in order to formulate more accurate entrainment and flow laws. However, while this data is being gathered and analyzed, it is essential that work continues on a model. Without a stable numerical tool, it will be difficult in future to interpret the incoming experimental results. Furthermore, as stated in the introduction, a well-tested, simple and reliable powder snow avalanche model is still missing in practice.

REFERENCES

Bartelt, P., Salm, B., & Gruber, U. (1999). Calculating dense-snow avalanche runout using a Voellmy fluid model with active/passive longitudinal straining. *J. Glaciol 45*(150), 242–254.

Fukushima, Y. & Parker, G. (1990). Numerical simulation of powder-snow avalanches. *J.Glaciol. 36*(123), 229–237.

Gruber, U. & Bartelt, P. (2000). Study of 1999 avalanches in Obergoms Valley, Switzerland with respect to avalanche hazard mapping. *Proc ISSW*.

Gruber, U. & Margreth, S. (2000). Winter 1999: A valuable test of avalanche hazard mapping procedure in Switzerland. *Ann. Glaciol 32*.

Hutter, K. (1996). Chapter 11: Avalanche dynamics. In V. Singh (Ed.), *The hydrology of disasters*, Dordrecht/Boston/London. Kluwer academic publishers.

Issler, D. (1998). Modelling of snow entrainment and deposition in powder-snow avalanches. *Ann. Glaciol. 26*, 253–258.

Keller, S. (1996). Physikalische Simulation von staublawinen. Mitteilungen 141, VAW.

Parker, G., Fukushima, Y., & Pantin, H. (1986). Self-accelerating turbidy currents. *J.Fluid Mech 171*, 145–181.

Sampl, P. (1998, Dec). The AVL quasi three- dimensional dense flow model. In C. Harbitz (Ed.), *EU Programme SAME : A Survey of Computational Models for Snow Avalanche Motion*, Oslo, pp. 67–69.

Sartoris, G. & Bartelt, P. (2000). Upwinded finite difference schemes for dense snow avalanche modelling. *Int. J. Numer. Meth. Fluids 32*, 799–821.

Savage, S. & Hutter, K. (1991). The dynamics of granular materials from initiation to runout. part i : Analysis. *Acta Mechanica* (86), 201–231.

Voellmy, A. (1955). Über die Zerstörungskraft von Lawinen. *Schweiz. Bauzeitung* (73), 159–165, 212–217, 246–249, 280–285.

APPENDIX

parameter	physical meaning	unit
t	Time	s
s	Track coordinate	m
z	Flow height coordinate	m
w	Track width	m
g	Gravitational acceleration	ms^{-2}
$\alpha(s)$	Slope angle	degree
$h_f(s,t)$	Flowing avalanche height	m
$h_p(s,t)$	Powder avalanche height	m
$\tilde{h}_f$	Flowing avalanche area ($\tilde{h}_f = h_f w$)	m
$\tilde{h}_p$	Powder avalanche area ($\tilde{h}_p = h_p w$)	m
ρ_f	Flowing avalanche density	kgm^{-3}
$\rho_p(s,t)$	Powder avalanche density	kgm^{-3}
$\rho_s(s)$	Density snowcover	kgm^{-3}
ρ_a	Density air	kgm^{-3}
ρ_i	Density ice	kgm^{-3}

parameter	physical meaning	unit
θ_a	Volumetric air content	
θ_i	Volumetric ice content	
$u_f(z,s,t)$	Velocity flowing avalanche	ms−1
$u_p(z,s,t)$	Velocity powder avalanche	ms−1
u_p'	Turbulent velocity fluctuations	ms−1
$U_f(s,t)$	Depth-averaged flowing velocity	ms−1
$U_p(s,t)$	Depth-averaged powder velocity	ms−1
$\dot{S}_a(s,t)$	Air entrainment volume rate	m^2s^{-1}
$\dot{S}_f(s,t)$	Flowing/powder volume exchange rate	m^2s^{-1}
$\dot{S}_e(s,t)$	Snowcover entrainment rate	m^2s^{-1}
$\dot{S}_c(s,t)$	Exchange rate stagnant/moving cloud	m^2s^{-1}
$\dot{S}_d(s,t)$	Deposition rate powder cloud	m^2s^{-1}
τ_b	Basal shear stress	Pa
τ_t	Turbulent drag (cloud)	Pa
$E_a(s,t)$	Air entrainment form factor	
$E_f(s,t)$	Flowing avalanche exchange factor	
$E_c(s,t)$	Stagnant cloud extrusion factor	
$E_s(s,t)$	Snowcover entrainment factor	
$T_e(s,t)$	Energy exchange factor	
$C_t(s,t)$	Turbulent drag factor	
$U_t(s,t)$	Threshhold shear velocity	ms^{-1}
μ	Dry-Coulomb friction flowing avalanche	
ξ	Velocity friction flowing avalanche	ms^{-2}
c	Cohesion	Pa
k	Active-Passive pressure coefficient	Pa
k_p	Passive pressure coefficient	Pa
k_a	Active pressure coefficient	Pa
λ	Pressure coefficient with cohesion	s^{-2}
β_1	Profile form factor	
β_2	Profile form factor	

Table 1: Definition of model parameters